Central European Journal of Energetic Materials
ISSN 1733-7178; e-ISSN 2353-1843

Cent. Eur. J. Energ. Mater. 2021, *18*(3): 322-338; DOI 10.22211/cejem/142488
Article is available in PDF-format, in colour, at:
https://ipo.lukasiewicz.gov.pl/wydawnictwa/cejem-woluminy/vol-18-nr-3/

Research paper

Effects of Metal Oxides on the Thermal Decomposition Kinetics and Mechanisms of HAN/PVA Based Propellants

Song-qi Hu[1)], **Xue-li Liu**[1)], **Lin-Lin Liu**[1,*)], **Bo Kang**[2)], **Yan Zhang**[1)]

[1)] *Science and Technology on Combustion, Internal Flow and Thermo-Structure Laboratory, Northwestern Polytechnical University, Xi'an 710072, P. R. China*
[2)] *Xi'an Changfeng Machinery and Electronics Institute, Xi'an 710065, P. R. China*
* *E-mail:* lll@nwpu.edu.cn

Abstract: The thermal decomposition processes of HAN/PVA-based propellants have been investigated using a simultaneous thermogravimetric analysis (TGA) – differential scanning calorimetry (DSC), coupled with Fourier-Transform Infrared Spectroscopy (FTIR) and Mass Spectrometry (MS) system. The activation energy (E_a), pre-exponential factor A and reaction mechanism function $f(\alpha)$ of the decomposition processes have been determined by non-isothermal and Malek methods. The results showed that the decomposition process of an HAN/PVA sample occurs mainly in the temperature range 202.2~220.1 °C, with a mass loss, heat release and E_a of about 84.8%, 1474.18 and 88.76 kJ·mol^{-1}, respectively. Of the seven metal oxides studied as catalysts, Al_2O_3, V_2O_5 and Fe_2O_3 have significant catalytic effects on an HAN/PVA-based propellant, in lowering the decomposition temperature, with E_a changing from 88.8 to 83.7, 85.6 and 113.6 kJ·mol^{-1}, respectively. The $f(\alpha)$ of both HAN/PVA and HAN/PVA/Al_2O_3 samples can be expressed as $f(\alpha) = (1 - \alpha)^2$, whereas $f(\alpha) = \alpha$ or $f(\alpha) = \alpha/2$ fit well for the HAN/PVA/V_2O_5 and HAN/PVA/Fe_2O_3 samples.

Keywords: HAN/PVA-based propellant, metal oxides, catalytic behaviour, kinetic parameters

1 Introduction

Hydroxylammonium nitrate (HAN) is widely studied as a raw material in non-toxic ionic liquid propellants and electrical solid propellants (ESP). For HAN-based propellants, this has the advantages of low freezing point, high density specific impulse, mild ablation with clean combustion products [1, 2]. Specifically for ESP with HAN as the oxidizer and water-soluble polyvinyl alcohol (PVA) polymer as the binder, this could improve the performance of solid rocket motors by providing restart and throttle capacity [3].

It should be noted that HAN/PVA-based propellants can also be used as conventional solid propellants due to the advantage of non-toxic and smokeless combustion products being produced. However, HAN/PVA-based propellants present difficulty on ignition and combustion due to the solvent water and the inert binder. The ignition and combustion processes always begin with thermal decomposition, and therefore the thermal decomposition mechanism is a key issue for HAN/PVA-based propellants.

In general, the decomposition mechanism of HAN is very complicated, and many studies indicate that the decomposition of solid HAN occurs at 180 °C with a proton transfer reaction, and there are also autocatalytic reactions for HAN solutions [4-7]. At present, the two main thermal decomposition mechanisms of HAN have been proposed by Oxley-Brower and Kelin (see [8, 9]). They believe that HAN initially undergoes a proton transfer reaction and forms hydroxylammonium and nitric acid. The products of the first step reaction then produce HNO and HONO with higher activity. Finally, the combustion products of HAN mainly include N_2O, N_2 and H_2O. The difference between the two mechanisms is that the N_2 and N_2O are produced by acid-catalyzed reactions as proposed by Kelin, whereas Oxley-Brower believes that NH_2OH reacts directly with HONO and HNO.

To improve the ignition and combustion performance of HAN-based propellants, there are a few reports on catalysts for HAN-based propellants [10-12]. Courthéoux prepared a catalyst bed based on alumina by using a sol-gel process with carbon dioxide supercritical drying and studied the effect of introducing 5 wt.% platinum metal. Kenji conducted the adsorption analysis by Monte Carlo Simulation to select metal catalysts for HAN and triethanolammonium nitrate (TEAN). The results showed that iridium is the best metallic catalyst [13-17].

Common combustion catalysts for solid propellants are mainly single metals, metal oxides and nanocomposites [18]. In the present study, HAN/PVA propellants with metal oxides as catalysts were prepared, and the thermal decomposition

process was studied by using a simultaneous TGA-DSC-FTIR-MS technique. The activation energy E_a, pre-exponential factor A and reaction mechanism function $f(\alpha)$ of the decomposition processes were determined.

2 Experimental

2.1 Materials

The materials used were:

- HAN, which was prepared by the metathesis reaction of barium nitrate and hydroxylammonium sulfate; the concentration of HAN solution was 80 wt.% after the distillation and concentration process.
- PVA (Chemically Pure), from Tianjin Kermel Chemical Reagent Co., Ltd.
- B_2O_3 (Analytical Reagent), from Tianjin Zhiyuan Reagent Co., Ltd.
- Al_2O_3 (Analytical Reagent), from Tianjin Hongyan Chemical Reagent Factory.
- V_2O_5 (Analytical Reagent), from Tianjin Yongsheng Fine Chemical Co., Ltd.
- Fe_2O_3 (Analytical Reagent), from Tianjin Fuchen Chemical Reagent Factory.
- Co_2O_3 (Analytical Reagent), from Tianjin Beilian Fine Chemicals Development Co., Ltd.
- Bi_2O_3 (Analytical Reagent), Chengdu Kelon Chemical Reagent Factory.

2.2 Preparation of the HAN/PVA solid propellant

According to the thermodynamic calculations, the highest specific impulse (I_{sp}) is reached at a chamber pressure of 5 MPa and a nozzle outlet pressure of 0.1 MPa when the mass ratio of HAN solution to PVA is 87:13, with an I_{sp} of 2083.4 $m \cdot s^{-1}$, and this ratio was therefore chosen for this study The HAN/PVA slurry was prepared by mixing granular PVA and the HAN solution at 67 °C for 1 h to ensure homogeneity of the mixture. The slurry containing a metal oxide catalyst was prepared by mixing 1 wt.% of the metal oxide and the HAN/PVA slurry at about 45 °C for 30 min. The samples were obtained after curing the slurry at 65 °C for 2 days.

2.3 Thermal analysis

A HAN/PVA sample of about 5 mg was heated in a simultaneous TGA-DSC (METTLER TOLEDO TGA/DSC1)-FTIR (Bruker Tensor27)-MS (PFEIFFER OMNI star) instrument from 40 to 700 °C at a heating rate of 10 $°C \cdot min^{-1}$. Samples of the HAN/PVA-based propellants (3 ±0.1 mg) were heated in a simultaneous TGA/DSC1 instrument from 35 to 350 °C under an argon atmosphere at heating rates of 5, 10, 15, and 25 $°C \cdot min^{-1}$, respectively.

3 Results and Discussion

3.1 Thermal decomposition process of the HAN/PVA sample

Figure 1 shows the TGA-DSC curves of the HAN/PVA sample at a heating rate of 10 °C·min^{-1}. It shows that the thermal decomposition of HAN/PVA sample could be divided into three stages, with cut-off points at 202.2 and 220.1 °C. The first stage may be attributed to evaporation of water in the sample due to a lower mass loss of about 4.9 wt.% without any significant heat flow effects. The second stage process occurs between 202.2~220.1 °C with a mass loss of 84.8% and heat release of 1474.18 J·g^{-1}, indicating violent thermal decomposition reactions of the HAN/PVA blend. There is only about 3 wt.% mass loss during the final stage, which may be caused by the further decomposition of incomplete condensed products from the second stage. There are still residues of 7 wt.% after the decomposition, and this should be carbon soot produced by the incomplete oxidation of PVA under the low oxidizer/fuel ratio.

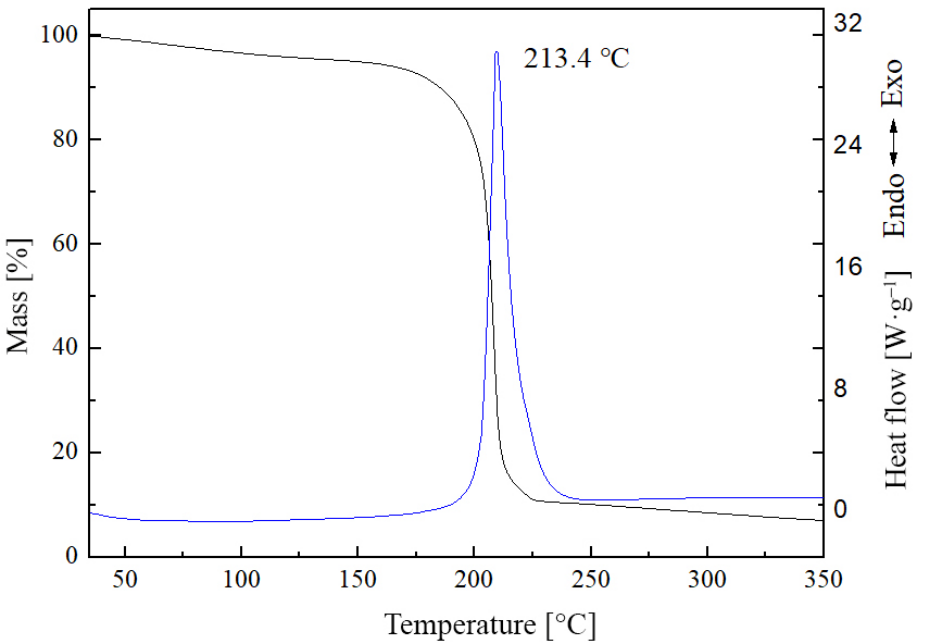

Figure 1. TGA-DSC curves of HAN/PVA propellant

The 3D FTIR and 3D MS spectra for the evolved gaseous decomposition products of the HAN/PVA sample are shown in Figures 2 and 3, respectively.

Figures 2 and 3 also indicate the violent decomposition reactions during the second stage, releasing a higher amount of gaseous products. The products are also more diverse than from the other stages. For the first stage, the weak peaks located at about 1500 and 3500 cm^{-1} in the FTIR spectra are attributed to $H_2O_{(g)}$, which agrees well with the results of the MS spectra. Therefore, evaporation of water in the HAN/PVA sample should be the rate-limiting part of the mass loss process during this stage. In addition, almost no effective signals for the products were detected in the third stage, indicating the very slow reactions with a trace amount of mass loss. These volatile products have much larger molecular weights, which are beyond the scope of the MS detector.

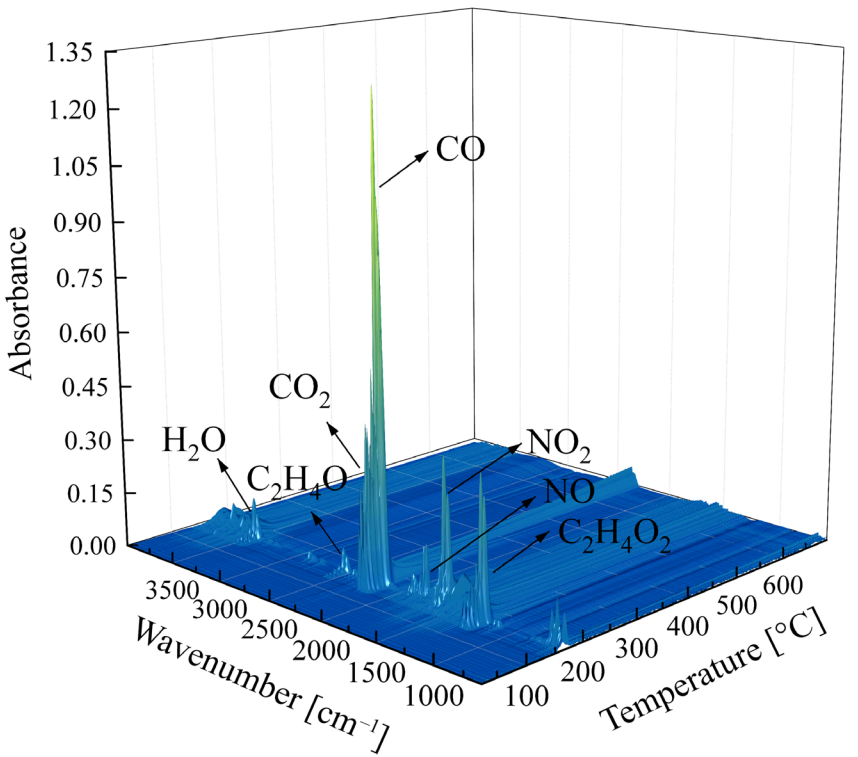

Figure 2. 3D FTIR spectrum

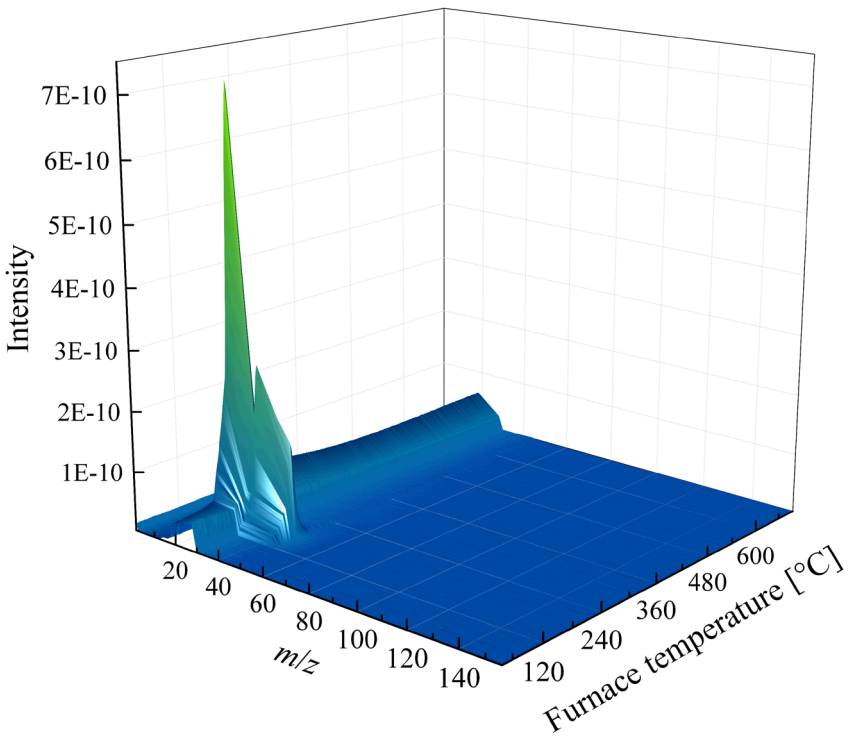

Figure 3. 3D MS spectrum

Considering the importance of the second stage and the similarity of the FTIR and MS curves under different temperatures during this stage, the 3D FTIR and 3D MS spectra with the highest absorbance and intensity were selected for investigation of the evolved gaseous products, as shown in Figures 4 and 5.

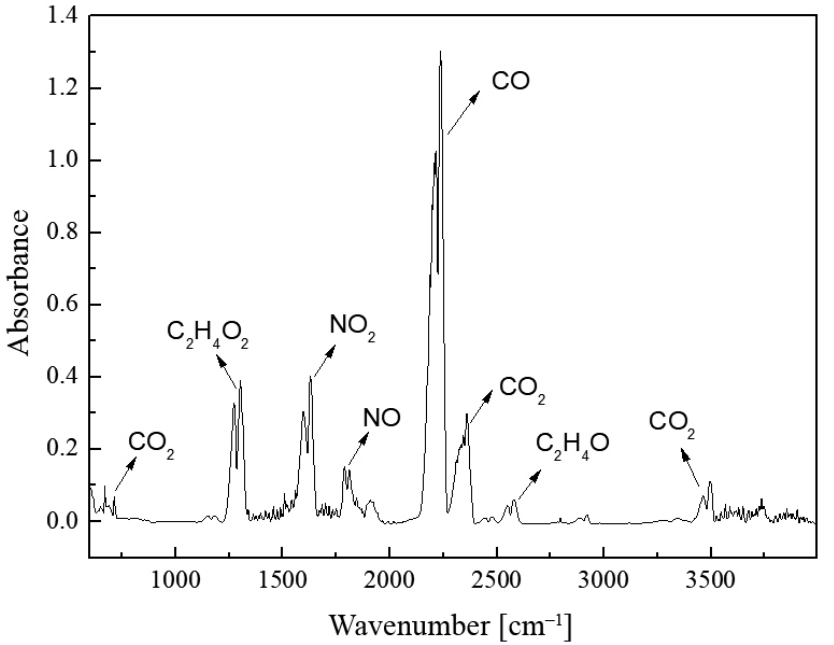

Figure 4. FTIR spectrum of the evolved gas at 166.6 °C

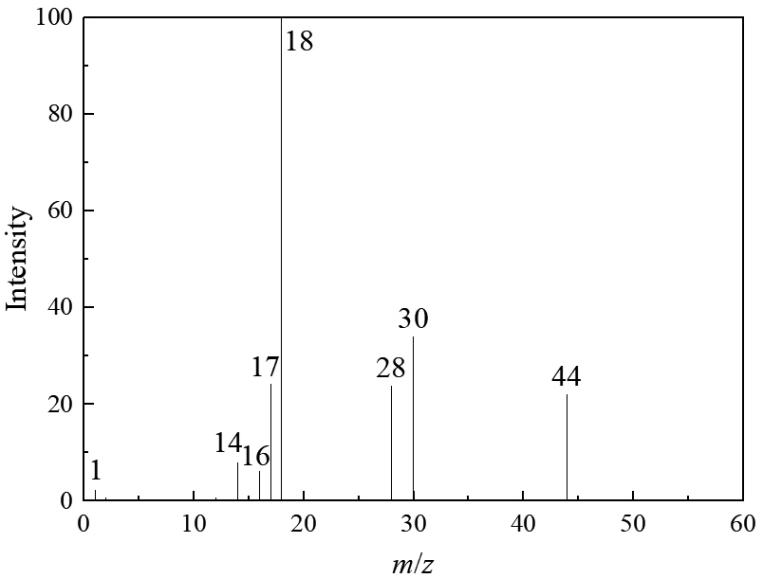

Figure 5. MS spectrum of the evolved gas at 163.3 °C

It can be seen from Figure 4 that the decomposition products are mainly CO, CO_2, NO, NO_2, C_2H_4O and $C_2H_4O_2$. The production of intermediate oxides such as CO and NO is attributed to the low oxidizer/fuel ratio of the composition, whereas the formation of C_2H_4O and $C_2H_4O_2$ is caused by the relatively low decomposition temperature. In addition, there were some peaks with very low absorbance, due to the presence of alcohols of low molecular weight, aldehydes or conjugated double bond polymers.

The mass spectra suggest that the decomposition products are mainly:

– H_2O (m/z = 17, 18),
– CO_2 (m/z = 16, 28, 44),
– CO (m/z = 28) and
– NO (m/z = 30),

which is consistent with the FTIR results in general. However, lesser products were detected by MS due to the limited capability of the equipment. In comparison to the products of pure HAN, which are HNO and HONO with higher activity, this indicates that HNO and HONO could be fully transformed to NO, NO_2 and H_2O, in the presence of PVA. The proton transfer reaction products of HAN oxidize PVA to CO, CO_2, C_2H_4O and $C_2H_4O_2$.

3.2 Thermal decomposition of HAN/PVA/metal oxide samples

Metal oxides including B_2O_3, Al_2O_3, V_2O_5, Fe_2O_3, Co_2O_3 and Bi_2O_3 were selected as the catalysts, and 1 wt.% of each of these metal oxides was added to the HAN/PVA mixture to improve the thermal decomposition rate. The TGA-DSC results of the samples at a heating rate of 10 °C·min^{-1} are shown in Figure 6 and the corresponding parameters are summarized in Table 1.

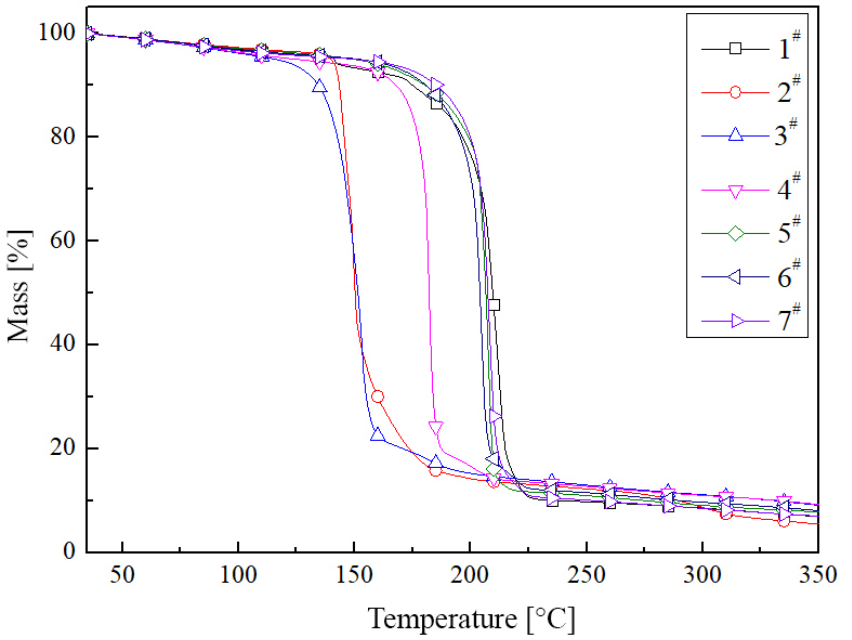

(a)

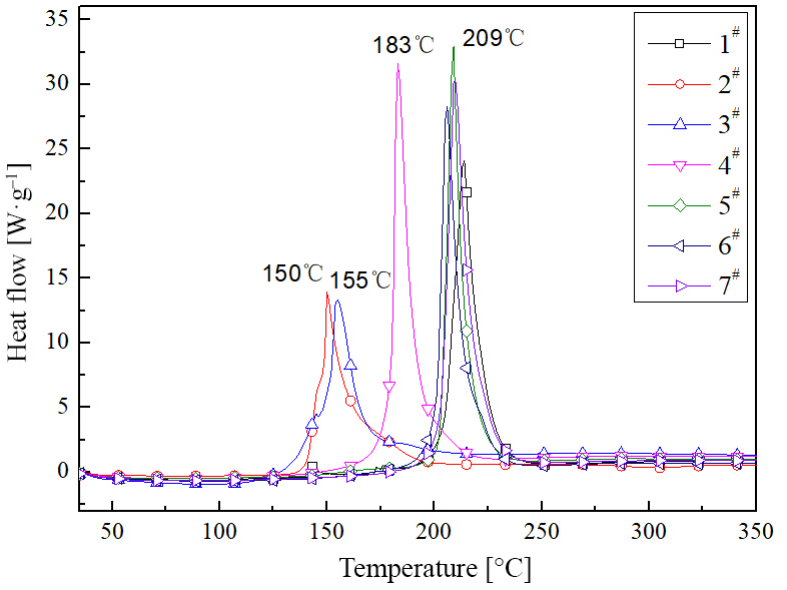

(b)

Figure 6. TGA-DSC curves of the HAN/PVA-based propellants

Table 1. Characteristic parameters of the samples

No.	Formulation	Onset temperature [°C]	Peak temperature [°C]	Endset temperature [°C]	Mass loss [%]	Heat release [J·g^{-1}]
1#	HAN/PVA/B_2O_3	204.3	217.39	223.29	78.85	1255.68
2#	HAN/PVA/Al_2O_3	145.1	150.28	158.12	77.25	938.99
3#	HAN/PVA/V_2O_5	148.7	154.95	165.37	70.83	992.84
4#	HAN/PVA/Fe_2O_3	178.8	187.11	192.06	77.33	1296.21
5#	HAN/PVA/Co_2O_3	202.4	213.70	216.16	79.84	1185.76
6#	HAN/PVA/Bi_2O_3	199.7	209.82	215.58	80.80	1229.10
7#	HAN/PVA	202.2	213.41	220.11	81.59	1438.82

Figure 6 and Table 1 indicate that Al_2O_3, V_2O_5 and Fe_2O_3 have the most significant catalytic effect on the thermal decomposition of HAN/PVA, resulting in a largely decreased decomposition temperature, by about 57.1, 53.5 and 23.4 °C respectively, which has a positive effect on increasing the burning rate of the propellant. However, the catalytic effect of Bi_2O_3 and Co_2O_3 is not obvious, and B_2O_3 even has a negative effect. Therefore, the study focused on Al_2O_3, V_2O_5 and Fe_2O_3, with more detail as follows, by investigating the catalytic reaction kinetic parameters.

3.3 Thermal decomposition kinetics of HAN/PVA propellants

The TGA curves could be easily converted into conversion rate and temperature relationship (α-*T*) curves, and then the temperature T_α corresponding to different α_i values in the α-T curves could be collected in increments of 0.05 in the range of $0.3 < \alpha < 0.8$. The activation energy E_α at the respective conversion rates α_i could be calculated by the iso-conversional method, and model-free methods, including the Flynn-Wall-Ozawa method, the Kissinger-Akahira-Sunose method and the Starink method, were used to evaluate E_a [19-22].

$$\ln(\beta) = \text{Const.-}1.052\left(\frac{E_a}{RT}\right) \tag{1}$$

$$\ln\left(\frac{\beta}{T^2}\right) = \text{Const.-}\frac{E_a}{RT} \tag{2}$$

$$\ln\left(\frac{\beta}{T^{1.92}}\right) = \text{Const.-}1.008\frac{E_a}{RT} \tag{3}$$

where β is the heating rate, E_α is the activation energy, and T is the temperature.

For the same conversion α_i and different heating rate β:
– the Flynn-Wall-Ozawa method fits a straight line with

$$\ln(\beta_i) - \frac{1}{T_i}, \tag{3a}$$

– the Kissinger-Akahira-Sunose method fits a straight line with

$$\ln\left(\frac{\beta_i}{T_i^2}\right) - \frac{1}{T_i}, \tag{3b}$$

– and the Starink method fits a straight line with

$$\ln\left(\frac{\beta_i}{T_i^{1.92}}\right) - \frac{1}{T_i}. \tag{3c}$$

Therefore, $E_{\alpha i}$ could be estimated from the slope of the lines (Equations 3a-3c). Figure 7 shows the relationship between E_α (estimated by the Starink method) and α for the propellant samples. Figure 7 shows that the activation energies are almost independent of the conversion for the four formulations in general, showing single reaction mechanisms governing the overall thermal decomposition process. Therefore, the mean value of E_a was used in this study as listed in Table 2.

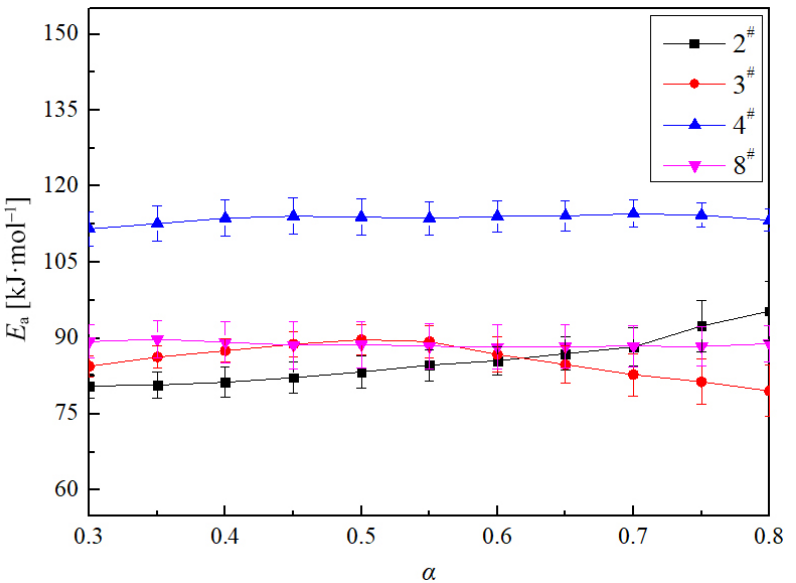

Figure 7. E_α-α curves estimated by the Starink method

Table 2. E_a obtained by the different methods

Sample No.	Formulation	E_a [kJ·mol^{-1}]		
		FWO	KAS	Starink
2#	HAN/PVA/Al_2O_3	86.0 ±2.5	83.5 ±2.6	83.7 ±2.6
3#	HAN/PVA/V_2O_5	87.8 ±3.0	85.4 ±3.2	85.6 ±3.2
4#	HAN/PVA/Fe_2O_3	115.0 ±0.8	113.4 ±0.8	113.6 ±0.8
7#	HAN/PVA	91.7 ±0.4	88.5 ±0.5	88.8 ±0.5

Table 2 shows that E_a values calculated by the three methods are similar with a relative error less than 4%, and the E_a calculated by the Starink method was then used in the following analysis. E_a decreased from 88.76 to 83.74 and 85.59 kJ·mol^{-1} respectively when Al_2O_3 and V_2O_5 were added. However, E_a increased after adding Fe_2O_3 even though the decomposition temperature decreased. The decomposition of solid HAN occurs at 180 °C with the proton transfer reaction, and the decreased decomposition temperature indicates that the presence of Fe_2O_3 would largely accelerate the proton transfer process, which is also the case for decomposition of AP [23]. However, Fe_2O_3 has no such catalytic effect on the decomposition of PVA, resulting in a higher apparent decomposition E_a. Also Fe_2O_3 has been reported to be very compatible with PVA and their combinations have been used in various studies [24]. Pure PVA without HAN would decompose at above 280 °C [25], hence the presence of Fe_2O_3 would decrease the oxidizing activity of HAN on PVA, and the decomposition of PVA would determine the overall apparent E_a.

3.4 Mechanism function for thermal decomposition of HAN/PVA propellants

The mechanism function $f(\alpha)$ of the decomposition reactions was determined by the Malek method [26, 27], and the $y(\alpha)$ and $Z(\alpha)$ functions obtained by a simple transformation of the non-isothermal data were the core points of the method.

$$\int_0^a \frac{d\alpha}{f(\alpha)} = G(\alpha) = \frac{ART^2}{E\beta}\exp(-\frac{E_a}{RT}) \tag{4}$$

The normalized $y(\alpha)$ expression could then be defined as:

$$y(\alpha) = (\frac{T}{T_{0.5}})^2 \frac{(\frac{d\alpha}{dt})}{(\frac{d\alpha}{dt})_{0.5}} = \frac{f(\alpha)G(\alpha)}{f(0.5)G(0.5)} \tag{5}$$

Similarly, the function of $Z(\alpha)$ can be formulated as follows [26]:

$$Z(\alpha) = f(\alpha)G(\alpha) = \frac{\pi(u)(\frac{d\alpha}{dt})T}{\beta} \tag{6}$$

where $\pi(u) = 1/(u + 2)$ is an approximation of the temperature integral, and $u = E_a/RT$ is the reduced activation energy. In addition, the pre-exponential factor A was calculated by the following equation [27]:

$$A = -\frac{\beta u_p}{T_p f'(\alpha_p)} e^{u_p} \tag{7}$$

where T_p is the peak temperature of the DSC curves, the subscript p referring to the peak.

The $y(\alpha)$-α and $Z(\alpha)$-α curves could be drawn by processing the TGA curves. Since the normalized $Z(\alpha)$-α and $y(\alpha)$-α curves are similar, only a comparison of the theoretical and experimental curves of $y(\alpha)$-α are given in this paper, and the results are shown in Figure 8 and Table 3.

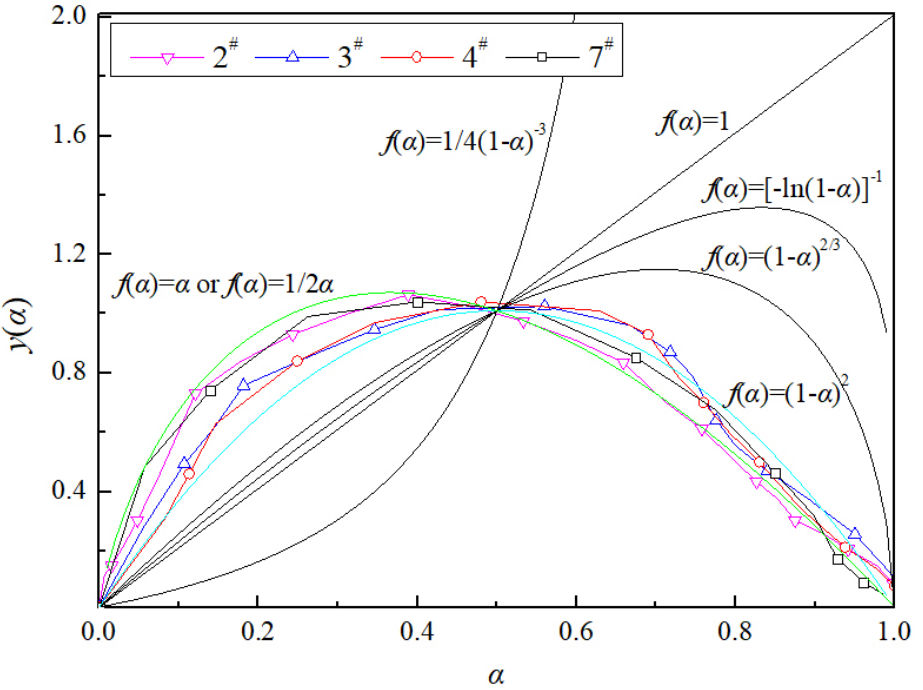

Figure 8. $y(\alpha)$-α curves (the curves without symbols are theoretical curves)

Table 3. $f(\alpha)$ and A of the samples

Sample	Formulation	$f(\alpha)$	A
2#	HAN/PVA/Al_2O_3	α or $(2\alpha)^{-1}$	$3.35\cdot10^8$ or $6.71\cdot10^8$
3#	HAN/PVA/V_2O_5	$(1-\alpha)^2$	$8.02\cdot10^{10}$
4#	HAN/PVA/Fe_2O_3	$(1-\alpha)^2$	$6.95\cdot10^{11}$
7#	HAN/PVA	α or $(2\alpha)^{-1}$	$4.35\cdot10^7$ or $8.69\cdot10^7$

Figure 8 indicates that the reaction mechanism function of both the HAN/PVA and HAN/PVA/Al_2O_3 samples is 1st or 2nd order of the exponential rule, $f(\alpha) = \alpha$ or $f(\alpha) = (2\alpha)^{-1}$, whereas it is $f(\alpha) = (1-\alpha)^2$ (2nd order chemical reaction model) for the samples using V_2O_5 and Fe_2O_3 as the catalysts. The changes in the pre-exponential factor are not obvious after the inclusion of Al_2O_3 and V_2O_5. However, Fe_2O_3 increases the pre-exponential factor by four orders of magnitude, which is consistent with an increase in E_a for this sample, according to the kinetic compensation effects rule for the same types of energetic materials with different additives [28].

The difference in mechanism function also suggests that the catalysts may take

effect by different routes. Through calculation, it was found that there is no kinetic compensation effect between the apparent E_a of the decomposition of the HAN/PVA based samples and the logarithm of the corresponding pre-exponential factor ($\ln A$), which may be due to the large number of hydroxyl groups in the PVA macromolecular chain. In the preparation of the samples, PVA has undergone coordination reactions and cross-linking reactions with Fe(III) or V(V). Therefore, the reaction of HAN oxidation of PVA is different from that of a simple HAN/PVA sample. In addition, when PVA was mixed with Fe_2O_3 or V_2O_5 only, V_2O_5 creates a degree of PVA cross-linking that is much less than that for Fe_2O_3, so the thermal decomposition temperature of the HAN/PVA/V_2O_5 sample is lower.

4 Conclusions

- The thermal decomposition of HAN/PVA samples could be divided into three stages, with the second stage, occurring between 202.2~220.1 °C, being dominant, with a mass loss, heat release and E_a of 84.8%, 1474.2 J·g^{-1} and 88.8 kJ·mol^{-1}, respectively. In addition, the gaseous decomposition products are mainly CO, CO_2, NO, NO_2, C_2H_4O and $C_2H_4O_2$.
- The metal oxides Al_2O_3, V_2O_5 and Fe_2O_3 have a significant catalytic effect on the decomposition of HAN/PVA, resulting in a lower decomposition temperature, and the E_a could be changed from 88.8 to 83.7, 85.6 and 113.6 kJ·mol^{-1} by adding 1 wt.% of Al_2O_3, V_2O_5 and Fe_2O_3 as catalysts, respectively.
- The most appropriate mechanism function for decomposition of HAN/PVA and HAN/PVA/Al_2O_3 samples is $f(\alpha) = \alpha$ or $f(\alpha) = (2\alpha)^{-1}$, whereas it is $f(\alpha) = (1 - \alpha)^2$ for the samples containing V_2O_5 and Fe_2O_3. The catalytic effect of Fe_2O_3 may be feasible due to the increase in the pre-exponential factor by four orders of magnitude.

Acknowledgements

This work was supported by the National Natural Science Foundation of China (Grant No. 51776175).

References

[1] Amrousse, R.; Katsumi, T.; Itouyama, N.; Azuma, N.; Kagawa, H.; Hatai, K.; Ikeda, H.; Hori, K. New HAN-based Mixtures for Reaction Control System and

Low Toxic Spacecraft Propulsion Subsystem: Thermal Decomposition and Possible Thruster Applications. *Combust. Flame* **2015**, *162*(6): 2686-2692.

[2] Baird, J.K.; Lang, J.R.; Hiatt, A.T.; Frederick, R.A. Electrolytic Combustion in the Polyvinyl Alcohol Plus Hydroxylammonium Nitrate Solid Propellant. *J. Propul. Power* **2017**, *33*(6): 1589-1590.

[3] Harikrishnan, E.S.; Hariharanath, B.; Vineeth, G.M.; Purushothaman, P. Thermokinetic Analysis and Performance Evaluation of Guanidinium Azotetrazolate Based Gas Generating Composition for Testing of Solid Rocket Motor Nozzle Closures. *Propellants Explos. Pyrotech.* **2018**, *43*(10): 1006-1012.

[4] Rafeev, V.; Rubtsov, Y.I. Kinetics and Mechanism of Thermal Decomposition of Hydroxylammonium Nitrate. *Russ. Chem. Bull.* **1993**, *42*(11): 1811-1815.

[5] Cronin, J.; Brill, T. Thermal Decomposition of Energetic Materials 29 – The Fast Thermal Decomposition Characteristics of a Multicomponent Material: Liquid Gun Propellant 1845. *Combust. Flame* **1988**, *74*(1): 81-89.

[6] Cronin, J.; Brill, T. Thermal Decomposition of Energetic Materials. 8. Evidence of an Oscillating Process during the High-rate Thermolysis of Hydroxylammonium Nitrate, and Comments on the Interionic Interactions. *J. Phys. Chem.* **1986**, *90*(1): 178-181.

[7] Van Dijk, C.A.; Priest, R.G. Thermal Decomposition of Hydroxylammonium Nitrate at Kilobar Pressures. *Combust. Flame* **1984**, *57*(1): 15-24.

[8] Khare, P.; Yang, V.; Meng, H.; Risha, G.A.; Yetter, R.A. Thermal and Electrolytic Decomposition and Ignition of HAN-Water Solutions. *Combust. Sci. Technol.* **2015**.

[9] Wei, C.; Rogers, W.J.; Mannan, M.S. Thermal Decomposition Hazard Evaluation of Hydroxylamine Nitrate. *J. Hazard. Mater.* **2006**, *130*(1): 163-168.

[10] Feng-Qi, Z. Preparation, Characterization and Combustion Catalytic Action of Bismuth/Zirconium Gallate. *Acta Phys.-Chim. Sin.* **2013**, *29*(4): 777-784(778).

[11] Vargeese, A.A.; Muralidharan, K. Kinetics and Mechanism of Hydrothermally Prepared Copper Oxide Nanorod Catalyzed Decomposition of Ammonium Nitrate. *Appl. Catal., A*. **2012**, *447-448*: 171-177.

[12] Wei, Z.-X.; Wang, Y.; Zhang, X.-J.; Hu, C.-W. Combustion Synthesis and Effect of $LaMnO_3$ and LaOCl Powder Mixture on HMX Thermal Decomposition. *Thermochim. Acta* **2010**, *499*(1-2): 111-116.

[13] Bao, L.; Zhang, W.; Zhang, X.; Chen, Y.; Chen, S.; Wu, L.; Shen, R.; Ye, Y. Impact of MWCNT/Al on the Combustion Behavior of Hydroxyl Ammonium Nitrate (HAN)-based Electrically Controlled Solid Propellant. *Combust. Flame* **2020**, *218*: 218-228.

[14] Courthéoux, L.; Popa, F.; Gautron, E.; Rossignol, S.; Kappenstein, C. Platinum Supported on Doped Alumina Catalysts for Propulsion Applications. Xerogels versus Aerogels. *J. Non-Cryst. Solids* **2004**, *350*: 113-119.

[15] Kappenstein, C.; Batonneau, Y.; Perianu, E.A.; Wingborg, N. Non Toxic Ionic Liquids as Hydrazine Substitutes. Comparison of Physico-Chemical Properties and Evaluation of ADN and HAN. *Eur. Space Agency Spec. Publ.* **2004**.

[16] Matsuo, T.; Mishima, H.; Hisatsune, K.; Katsumi, T.; Sawai, S.; Hori, K.

Development of HAN-based Liquid Propellant Thruster. *Int. J. Energ. Mater. Chem. Propul.* **2008**, *7*(2): 139-152.

[17] Popa, A.F.; Courthéoux, L.; Gautron, E.; Rossignol, S.; Kappenstein, C. Aerogel and Xerogel Catalysts Based on θ-Alumina Doped with Silicon for High Temperature Reactions. *Eur. J. Inorg. Chem.* **2005**, *2005*(3): 543-554.

[18] Yan, Q.-L.; Zhao, F.-Q.; Kuo, K.K.; Zhang, X.-H.; Zeman, S.; DeLuca, L.T. Catalytic Effects of nano Additives on Decomposition and Combustion of RDX-, HMX-, and AP-based Energetic Compositions. *Prog. Energy Combust. Sci.* **2016**, *57*: 75-136.

[19] Akahira, T.; Sunose, T. Method of Determining Activation Deterioration Constant of Electrical Insulating Materials. *Res. Rep. Chiba Inst. Technol.* **1971**, *16*: 22-23.

[20] Flynn, J.H.; Wall, L.A. General Treatment of the Thermogravimetry of Polymers. *J. Res. Natl. Bur. Stand., Sect. A*. **1966**, *70A*(6): 487-523.

[21] Starink, M.J. The Determination of Activation Energy from Linear Heating Rate Experiments: a Comparison of the Accuracy of Isoconversion Methods. *Thermochim. Acta* **2003**, *404*(1): 163-176.

[22] Vyazovkin, S.; Burnham, A.K.; Criado, J.M.; Pérez-Maqueda, L.A.; Popescu, C.; Sbirrazzuoli, N. ICTAC Kinetics Committee Recommendations for Performing Kinetic Computations on Thermal Analysis Data. *Thermochim. Acta* **2011**, *520*(1): 1-19.

[23] Ma, Z.; Li, F.; Bai, H. Effect of Fe_2O_3 in Fe_2O_3/AP Composite Particles on Thermal Decomposition of AP and on Burning Rate of the Composite Propellant. *Propellants Explos. Pyrotech.* **2010**, *31*(6): 447-451.

[24] Bulinski, M.; Kuncser, V.; Plapcianu, C.; Krautwald, S.; Franke, H.; Rotaru, P.; Filoti, G. Optical and Electronic Properties of Polyvinyl Alcohol Doped with Pairs of Mixed Valence Metal Ions. *J. Phys. D Appl. Phys.* **2004**, *37*(17): 2437-2441.

[25] Peng, Z.; Kong, L.X. A Thermal Degradation Mechanism of Polyvinyl Alcohol/Silica Nanocomposites. *Polym. Degrad. Stab.* **2007**, *92*(6): 1061-1071.

[26] Šesták, J.; Málek, J. Diagnostic Limits of Phenomenological Models of Heterogeneous Reactions and Thermal Analysis Kinetics. *Solid State Ionics* **1993**, *63-65*: 245-254.

[27] Málek, J. The Kinetic Analysis of non-Isothermal Data. *Thermochim. Acta* **1992**, *200*: 257-269.

[28] Yan, Q.-L.; Zeman, S.; Zhang, J.-G.; Qi, X.-F.; Li, T.; Musil, T. Multistep Thermolysis Mechanisms of Azido-s-triazine Derivatives and Kinetic Compensation Effects for the Rate-Limiting Processes. *J. Phys. Chem. C*. **2015**, *119*(27): 14861-14872.

Received: October 12, 2020
Revised: September 21, 2021
First published online: September 30, 2021